Check for updates

HDAC-6 inhibition ameliorates the early neuropathology in a mouse model of Krabbe disease

Sandra O. Braz[1†], Marlene M. Morgado[1†], Marta I. Pereira[1],
Ana C. Monteiro[1], Olga Golonzhka[2], Matthew Jarpe[2],
Pedro Brites[3], Monica M. Sousa[1]* and
Joana Nogueira-Rodrigues[1]*

[1]Nerve Regeneration Group, Instituto de Biologia Molecular e Celular (IBMC), Instituto de Investigação e Inovação em Saúde (i3S), University of Porto, Porto, Portugal, [2]Acetylon Pharmaceuticals Inc., Boston, MA, United States, [3]NeuroLipid Biology Group, Instituto de Biologia Molecular e Celular (IBMC), Instituto de Investigação e Inovação em Saúde (i3S), University of Porto, Porto, Portugal

Introduction: In Krabbe disease (KD), mutations in β-galactosylceramidase (GALC), a lysosomal enzyme responsible for the catabolism of galactolipids, leads to the accumulation of its substrates galactocerebroside and psychosine. This neurologic condition is characterized by a severe and progressive demyelination together with neuron-autonomous defects and degeneration. Twitcher mice mimic the infantile form of KD, which is the most common form of the human disease. The Twitcher CNS and PNS present demyelination, axonal loss and neuronal defects including decreased levels of acetylated tubulin, decreased microtubule stability and impaired axonal transport.

Methods: We tested whether inhibiting the α-tubulin deacetylase HDAC6 with a specific inhibitor, ACY-738, was able to counteract the early neuropathology and neuronal defects of Twitcher mice.

Results: Our data show that delivery of ACY-738 corrects the low levels of acetylated tubulin in the Twitcher nervous system. Furthermore, it reverts the loss myelinated axons in the sciatic nerve and in the optic nerve when administered from birth to postnatal day 9, suggesting that the drug holds neuroprotective properties. The extended delivery of ACY-738 to Twitcher mice delayed axonal degeneration in the CNS and ameliorated the general presentation of the disease. ACY-738 was effective in rescuing neuronal defects of Twitcher neurons, stabilizing microtubule dynamics and increasing the axonal transport of mitochondria.

Discussion: Overall, our results support that ACY-738 has a neuroprotective effect in KD and should be considered as an add-on therapy combined with strategies targeting metabolic correction.

KEYWORDS

axonal transport, HDAC6, Krabbe disease, leukodystrophy, microtubule stability, tubulin acetylation, Twitcher mice

1. Introduction

Krabbe disease (KD), or globoid cell leukodystrophy, is a lysosomal storage disorder caused by mutations in the *galc* gene that result in impaired activity of the lysosomal hydrolase galactosylceramidase (GALC). As a consequence of GALC deficiency, the metabolism of several galactosphingolipids is impaired and GALC substrates - galactosylceramide and

galactosylsphingosine (also known as psychosine), accumulate (Wenger et al., 1997). Whereas galactocerebroside builds up inside macrophages and microglia giving rise to globoid cells, psychosine is highly toxic to myelin-forming cells (oligodendrocytes in the central nervous system - CNS - and Schwann cells in the peripheral nervous system - PNS). Psychosine disrupts the architecture and composition of lipid rafts (White et al., 2009) and leads to the activation of apoptosis pathways that result in progressive demyelination (Krabbe, 1916; Miyatake and Suzuki, 1972; Igisu and Suzuki, 1984; Zaka and Wenger, 2004). Consequently, KD patients present severe irritability, limb stiffness, motor function impairment, mental development arrest, epileptic seizures, hypertonicity and dystonia (Krabbe, 1916; Bradbury et al., 2021). Among the KD onsets based on the age of presentation of symptoms, the infantile onset is the most prevalent and severe subtype, as patients usually do not survive past 2 years of age (Hagberg et al., 1969; Bradbury et al., 2021). The Twitcher mouse, a naturally occurring mutant with a premature stop codon in the *galc* gene that results in lack of functional GALC (Suzuki and Suzuki, 1995), mimics the infantile form of KD (Lee et al., 2006). Similarly to human patients, Twitcher mice present demyelination both in the CNS and PNS that can be clearly detected at post-natal day 15 (P15) (Tanaka et al., 1988).

Hematopoietic stem cell transplantation (HSCT) emerged as one of the most valuable treatments for KD, delaying disease progression and extending life time of KD patients if transplantation is performed before the onset of symptoms (Escolar et al., 2005; Kreher et al., 2022). In spite of co-morbidities, HSCT slows down disease progression and improves pathology in the CNS, while a less significant effect is observed in the PNS, possibly given the lower ability of Schwann cells to uptake exogenous GALC (Wright et al., 2017; Weinstock et al., 2020; Kofler et al., 2022). Two AAV-based clinical trials for KD (NCT04693598 and NCT04771416) are currently underway (Heller et al., 2023) but, it is likely that future therapeutic approaches for KD will rely on combinatorial strategies aimed at providing the missing enzyme and simultaneously counteract neuroinflammation and promote neuroprotection.

With respect to neuroprotection, it is important to note that in addition to demyelination, neuronal-autonomous defects are also central players in KD progression (Nogueira-Rodrigues et al., 2016; Brites and Sousa, 2022; Kreher et al., 2022). In fact, a myelin-independent axonopathy contributes to the severe neuropathology in Twitcher mice (Castelvetri et al., 2011; Smith et al., 2011; Teixeira et al., 2014; Kreher et al., 2022), correlating with reports of loss of unmyelinated axons in human KD nerves (Sourander and Olsson, 1968). Our group has shown that before the onset of demyelination, Twitcher mice already exhibit a decreased number of axons in the CNS and PNS, and of sensory neurons in dorsal root ganglia (Teixeira et al., 2014). In fact, Twitcher neurons have a generalized impairment in axonal transport including mitochondria (Cantuti Castelvetri et al., 2013), lysosomes (Teixeira et al., 2014) and synaptic vesicles (Teixeira et al., 2014), possibly associated with abnormal levels of post-translational modifications of tubulin and with a decreased microtubule stability (Teixeira et al., 2014). Of note, in Twitcher mice, microtubules have decreased levels of polyglutamylated and acetylated tubulin (Teixeira et al., 2014), which may be directly linked with the defective axonal transport.

α-Tubulin acetylation is tightly regulated by α-tubulin-acetyltransferases (αTATs) and a specific histone deacetylase, HDAC6, that has a cytoplasmic location and thereby does not interfere with histone acetylation (Hubbert et al., 2002). Studies using HDAC6 inhibitors highlighted their neuroprotective role as they facilitate axonal transport by promoting microtubule acetylation (Dompierre et al., 2007; Rivieccio et al., 2009; Zilberman et al., 2009; Chen et al., 2010). This is especially relevant in KD, as Twitcher mice have impaired axonal transport and diminished levels of acetylated tubulin (Teixeira et al., 2014). Several HDAC6 inhibitors have been used in various models of neurodegeneration such as tubastatin A (Jian et al., 2017), trichostatin A (Su et al., 2021), ACY-775 (Benoy et al., 2017) and ACY-738 (Rossaert et al., 2019). ACY-738 (N-hydroxy-2-(1-phenylcycloproylamino)pyrimidine-5-carboxamide) inhibits the C-terminal catalytic domain of HDAC6, increasing α-tubulin acetylation without altering histone acetylation (Jochems et al., 2014). ACY-738 has low nanomolar potency (IC$_{50}$–1,7 nM) with a high selectivity of 60-1,500-fold over class I HDACs. Although this compound has a rapid elimination from plasma (T$_{1/2}$–0.2 h), upon systemic administration, it leads to a ratio brain-plasma exposure of 1.22:1, demonstrating a higher capacity to cross the blood–brain barrier than other HDAC6 inhibitors such as tubastatin A (Jochems et al., 2014; Majid et al., 2015). As stable microtubules are the railroads for axonal cargos, ACY-738 is also associated with increased efficiency of axonal transport (Majid et al., 2015; Guo et al., 2017). Current data indicates that ACY-738 promotes axon growth *in vitro* in inhibitory conditions (Rivieccio et al., 2009), and *in vivo* improves the outcome of animal models of several neurodegenerative conditions, including Alzheimer's disease, multiple sclerosis, Charcot–Marie-Tooth and amyotrophic lateral sclerosis. In mouse models of demyelinating disorders, such as multiple sclerosis, ACY-738 treatment increases short-term memory and decelerates disease progression (LoPresti, 2019), whereas in a model of Charcot–Marie–Tooth disease (a demyelinating neuropathy), ACY-738 improves sensory and motor nerve conduction (Benoy et al., 2017). In the case of Amyotrophic Lateral Sclerosis, treating the TgFUS$^{+/+}$ mouse model with ACY-738 leads to improved axonal transport, motor phenotypes and lifespan (Rossaert et al., 2019; Burg et al., 2021). ACY-738 has been shown to ameliorate Alzheimer disease' related-impairments such as short term memory and hyperactivity, by acting on tau and tubulin modifications leading to normalization of axonal transport (Majid et al., 2015). In view of the therapeutic properties of ACY-738 in conditions that share similar pathological features to Krabbe disease, including demyelination and axonal transport defects, it emerged as a promising candidate to test in this leukodystrophy.

Given the impairment caused by the defect in tubulin acetylation in Twitcher nerves, we tested whether ACY-738 delivery could counteract the early neuropathology of this KD model. Here, we show that the early systemic delivery of ACY-738 robustly increases tubulin acetylation, stabilizes microtubule dynamics, increases axonal transport, and rescues the early loss of myelinated axons in the optic and sciatic nerves of Twitcher mice. Our results thus support that ACY-738 has neuroprotective effect in KD and should be considered as an add-on therapy in KD.

2. Materials and methods

2.1. Animals

Twitcher (twi) mice and wild-type (WT) littermates were obtained from heterozygous breeding pairs (Jackson Laboratory). Genotyping

of Twitcher mice was based on the use of a PCR mismatched primer that creates a restriction site for EcoRV if the *Galc* allele possesses the mutation, as described (Sakai et al., 1996). Mice were bred at the i3S animal facility with *ad libitum* access to water and rodent food, and were kept on a 12 h light and dark cycle. All mice were handled and euthanized according to the i3S humane endpoints standard operation procedure established according to FELASA's recommendations[1] when any of the following features was observed: persistent lethargy and paralysis, severely impaired mobility, prolonged dehydration (for more than 72 h) or severe weight loss (more than 20%) arising from inability of drinking or eating. After weaning, Twitcher mice were fed with accessible wet rodent's chow and supplemented with Anima-Strath. Animals were euthanized either at P9 or humane endpoints. The time-point P9 was chosen given that axonal loss can be detected readily at this time point, prior to the onset of demyelination and associated phenotypes (Teixeira et al., 2014), allowing to distinguish the effects of ACY-738 treatment on axonal intrinsic defects.

2.2. Functional evaluation

Animals were monitored twice per week until P25 and then daily until humane endpoints were reached. Parameters including weight loss, natural/provoked behavior, and activity level were scored. Natural behavior was assessed by observation of the animals in their home cage; animals with normal behaviour, i.e., moving, grooming and feeding, and alert received the highest score 3, animals with minor changes to these parameters were scored as 2, animals with severely decreased mobility but that were still alert received a score of 1, whereas less motile and not alert animals scored 0. The animals were then touched to provoke a response, which was scored with 3 if the animal reacted normally (i.e., escaping and freezing), 2 if minor changes to normal behavior were found, 1 if moderate changes to the escaping and freezing responses were seen or 0 is the escaping and freezing responses were absent. Activity level was evaluated by observation of the animals in their home cage during 5 min and recording the time spent ambulating and exploring; animals active for more than 4 min received the highest score (3), and animals with less than 1 min of activity scored (0). Twitching frequency was accessed also twice a week using a similar scoring system, with animals with rare twitching scoring 4 and animals with severe tremors soring 1.

2.3. Subcutaneous delivery of ACY-738

ACY-738 (Acetylon Pharmaceuticals) was prepared in 0.5% hydroxypropyl methylcellulose (HPMC) diluted in PBS at a final concentration of 0.5 mg/mL. Starting at P0, Twitcher mice were injected subcutaneously every day (3 mg/kg) with either ACY-738 (in 0.5% HPMC) or vehicle (0.5% HPMC) and euthanized at P9 ($n = 10$ for each condition) or maintained until humane endpoints were reached ($n = 10$–14 animals for each condition). WT mice were also injected subcutaneously daily with ACY-738 ($n = 8$–10) or vehicle ($n = 8$–10) to serve as controls. Either at P9 or when animals reached

humane endpoints, brains, sciatic nerves, optic nerves and dorsal root ganglia (DRG) were collected and processed for morphometric analysis, western blot analysis or primary neuron cultures, as described below. During the delivery period, no signs of toxicity of the drug were detected.

2.4. Western blot analysis

Sciatic nerves, optic nerves and brains from ACY-738-treated Twitcher mice ($n = 10$) or control Twitcher mice ($n = 8$–9) were homogenized in lysis buffer (PBS containing 0.3% Triton X-100), 1 mM sodium orthovanadate and protease inhibitors (Roche, 4693132001). Total protein of each sample was determined using the Bio-Rad DC kit (Bio-Rad, 5000116) and protein lysates were run on 10% SDS-PAGE (5 μg/lane) and transferred to supported nitrocellulose membranes (Amersham, 10600013). Membranes were incubated overnight at 4°C with mouse anti-acetylated tubulin (1:20,000; Sigma, T7451), rat anti-tyrosinated tubulin (clone YL1/2, 1:2000; Bio-Rad, MCA77G) and mouse anti-α-tubulin (1:10,000; Sigma, T6199). Given the difficulty to perform stripping of anti-tubulin antibodies from the membranes, two separated gels were loaded and transferred simultaneously to probe for either acetylated- or α-tubulin. Secondary antibodies were HRP-conjugated anti-mouse IgG (1:5,000; Jackson ImmunoResearch, 115-035-003) or the IRDye® 800CW Goat anti-Mouse IgG (1:5,000; LI-COR, 926-32,210). Proteins were detected using Luminata Forte (Millipore, WBLUR0500) and quantification was performed by densitometry using QuantityOne software (Bio-Rad). Alternatively, the Odyssey CLx (LI-COR) imaging system was used for detection of membrane total protein (926-11,010) and dye-conjugated labelled secondary antibodies (926-32,212 and 926-68,073).

2.5. Neuropathological analysis

For each animal (both in the case of ACY-738 delivery from P0 to P9 and from P0) until humane endpoints ($n = 8$ ACY-738-treated and $n = 8$ control Twitcher mice), the right sciatic and optic nerves were used for neuropathological analyses. All tissues were isolated and fixed by immersion in 4% glutaraldehyde in 0.1 M sodium cacodylate buffer (pH 7.4) for 5 days and processed for electronic microscopy as previously described (da Silva et al., 2014). Briefly, the tissues were submitted to postfixation with 1% OsO4 in 0.1 M cacodylate buffer (pH 7.4) for 2 h, after which they were dehydrated and embedded in Epon (Electron Microscopy Sciences). To determine the number of myelinated axons, 1 μm-thick transverse sections covering the complete cross-sectional area of the sciatic nerve were stained with p-phenylene-diamine (PPD) and the total number of myelinated axons was counted. For g-ratio analysis, the axonal diameter and the myelin sheath thickness were measured by dividing the diameter of each axon by its myelin-including diameter (80–150 fibers per animal). To determine the density of unmyelinated axons, ultrathin transverse sciatic nerve sections (50 nm) were cut, stained with uranyl acetate and lead citrate and 10 non-overlapping photomicrographs (5,000× magnification) were taken in a transmission electron microscope (JEOL 100CX II). The optic nerve was treated similarly and myelinated and unmyelinated axons were counted from ultrathin transverse nerve

sections. In all measurements, the observer was blinded to the experimental condition.

2.6. Primary culture of dorsal root ganglia neurons

DRG were isolated from WT and Twitcher mice at P9 or when humane endpoints were reached. Ganglia were collected to DMEM:F12 (Sigma-Aldrich, D8437) supplemented with 10% fetal bovine serum (FBS; Sigma-Aldrich, F9665) and 1% penicillin/ streptomycin (P/S; Invitrogen, 15,140–122). DRG were digested with collagenase IV-S (Sigma-Aldrich, C1889) for 1 h and 30 min. Neurons were isolated centrifuging the cell suspension into a 15% bovine serum albumin (BSA; Sigma-Aldrich, A3294) cushion, for 10 min at 1000 rpm. Cells were resuspended in DMEM:F12 supplemented with 1% P/S, 2× B27 (Invitrogen, 0080085SA), 2 mM L-glutamine (L-Glu; Invitrogen, 25,030,024) and 50 ng/mL nerve growth factor (NGF; Merck Millipore, 01-125).

2.7. Assessment of microtubule dynamics

For the analysis of microtubule dynamics in the growth cone, DRG neurons from Twitcher and WT mice from animals euthanized humane endpoints were isolated as described above and nucleofected with a plasmid encoding pEGFP-eEB3 (Addgene #190164). After transfection, cells were left in suspension for 24 h. At DIV1, cells were plated at a density of 10,000 cells/well in glass-bottom 8-well μ-dishes. At DIV5, 2 h before imaging, half of the medium was replaced with complete media without phenol red and supplemented with 100 nM ACY-738 in 0.1% DMSO or 0.1% DMSO alone. Transfected cells were visualized using the 100x objective of a spinning disk confocal system Andor Revolution XD with an iXonEM+ DU-897 camera and IQ 1.10.1 software (ANDOR Technology). Time-lapse recordings (a total of 60 frames, every 2 s) were acquired in three planes separated by 0.2 μm each at 37°C and 5% CO2. For the quantification of EB3 comet growth speed, kymographs were performed using the Fiji KymoResliceWide plugin (distance, x axis; time, y axis). Starting and end positions of the traces were defined using the Fiji Cell Counter plugin.

2.8. Analysis of axonal transport

For live imaging of axonal transport, DRG neurons from ACY-738-treated and control mice were isolated as previously described from animals euthanized at humane endpoints. Dissociated DRG neurons (4,000 cells/well) were cultured in DMEM:F12 supplemented with NGF, Pen/Strep, B27 and L-glutamine for 16 h in 8-well μ-slides ibiTreat (Ibidi) coated with PLL and laminin. DRG neurons isolated from ACY-738-treated WT and Twitcher mice were maintained in culture in the presence of 100 nM ACY-738 in 0.1% DMSO. Control WT and Twitcher DRG neurons were maintained in 0.1% DMSO. For the analysis of axonal transport of mitochondria, DRG neurons were incubated with Mitotracker (Invitrogen, M7510) in DMEM:F12 for 45 min at 37°C. Axonal transport was visualized in a confocal SP5II Leica microscope. Photomicrographs were taken for

2 min with 1 s frame intervals with 5 Z-stacks per frame. For each condition, the movement of at least 50 organelles was tracked. Analysis of axonal transport (velocity and flux) was done using the Fiji software.

2.9. Quantification and statistical analysis

Data is shown as mean and standard error of the mean (SEM). The statistical analysis for all experiments was performed with GraphPad Prism 9. Unless elsewhere stated, the following statistical tests were used as indicated in figure legends: two-tailed unpaired t-test, one-way or two-way ANOVA followed by multiple comparison tests or Welch ANOVA test if unequal variances were observed between the groups. Sample sizes are indicated in figure legends and significance was defined as p value* < 0.05, p** < 0.01, p*** < 0.001, p**** < 0.0001, ns: not significant.

3. Results

3.1. ACY-738 subcutaneous delivery increases tubulin acetylation in the nervous tissue of Twitcher mice

To test the possible neuroprotective effect of ACY-738 in KD, the drug was delivered subcutaneously daily to Twitcher mice. Since Twitcher mice present axonal loss that can be detected readily at P9, prior to the onset of demyelination (Teixeira et al., 2014), we explored the potential beneficial effects of ACY-738 delivery from P0 to P9 (Figure 1A). We analyzed the levels of tubulin acetylation in brains, optic and sciatic nerves from P9 ACY-738-treated Twitcher mice. As expected from the capacity of ACY-738 to penetrate the nervous system (Jochems et al., 2014), all tissues had increased levels of acetylated tubulin in ACY-738-treated Twitcher mice (9-, 2- and 4-fold, respectively; Figures 1B–D). No differences were seen in the levels of other tubulin modifications including tyrosinated tubulin resulting from ACY-738 treatment (Supplementary Figure S1A). We then extended our analysis of ACY-738 effect on Twitcher mice treated until humane endpoints were reached (Figure 1E). At this timepoint, untreated Twitcher mice had decreased levels of acetylated tubulin in the brain (Figure 1F) and optic nerve (Figure 1G). In the sciatic nerve, in support of our previous observations at P9 (Teixeira et al., 2014), at humane endpoints a tendency for decreased tubulin acetylation in Twitcher mice persisted (Figure 1H). ACY-738 treatment resulted in increased tubulin acetylation in all the examined tissues of Twitcher mice (Figures 1F,G). Collectively our data show that Twitcher mice have decreased acetylated tubulin levels throughout the nervous system that can be reverted by ACY-738 systemic delivery.

3.2. ACY-738 stabilizes microtubule dynamics and increases the axonal transport of mitochondria in Twitcher DRG neurons

Twitcher neurons exhibit decreased acetylated tubulin levels, decreased microtubule cytoskeleton stability (Teixeira et al., 2014),
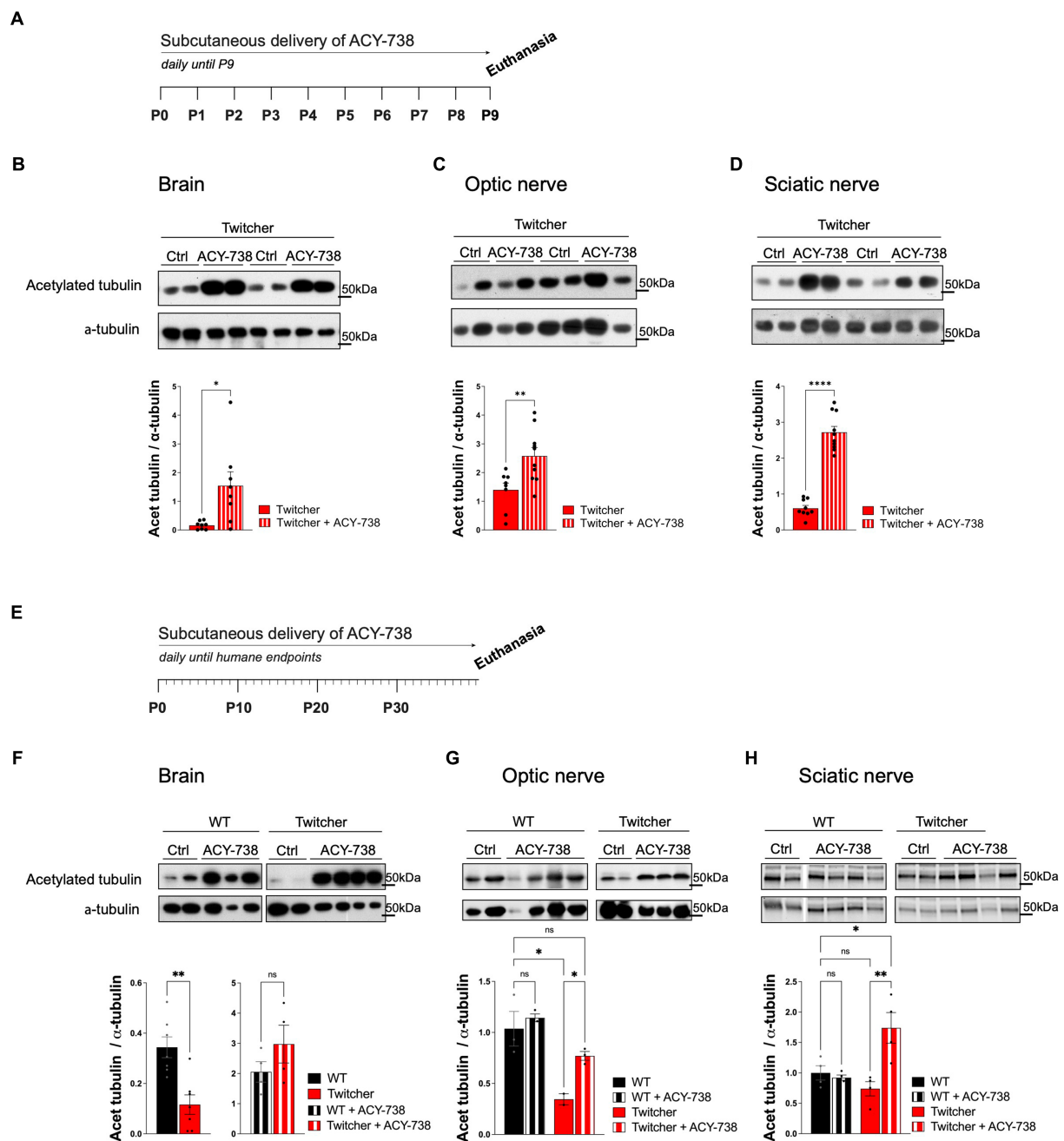
FIGURE 1
Western blot analysis of tissues from WT and Twitcher mice treated with ACY-738 from P0 until P9 or until and humane endpoints. **(A)** Timeline of the experimental set-up of daily ACY-738 delivery from P0 to P9. **(B–D)** Western blot analysis of acetylated tubulin and α-tubulin in **(B)** brains, **(C)** optic nerves and **(D)** sciatic nerves of P9 WT and Twitcher mice untreated or treated with ACY-738 (upper panels) and respective quantifications (lower panels). Data represent mean $\pm$ SEM (*$p < 0.05$, **$p < 0.01$, ****$p < 0.0001$, two-tailed unpaired t-test) of $n = 8–9$ control Twitcher and $n = 8–10$ ACY-738-treated Twitcher. **(E)** Timeline of the experimental set-up of daily ACY-738 delivery from P0 until humane endpoints. **(F–H)** Western blot analysis of acetylated tubulin and α-tubulin of **(F)** brains, **(G)** optic nerves and **(H)** sciatic nerves of WT and Twitcher mice untreated and treated with ACY-738 until humane endpoints were reached (upper panels) and respective quantifications (lower panels). Data represent mean $\pm$ SEM (*$p < 0.05$, **$p < 0.01$, one-way ANOVA followed by Welch's correction or Tukey's multiple comparison test). Note that in the case of the brain **(F)**, given the differences in treated and untreated animals, quantification in separate gels was done for untreated WT and Twitcher mice. Data represent mean $\pm$ SEM (**$p < 0.01$, two-tailed unpaired t-test) of $n = 3–4$ control WT mice, $n = 4$ ACY-738-treated WT mice, $n = 2–4$ control Twitcher and $n = 4$ ACY-738-treated Twitcher.

and impaired axonal transport (Cantuti Castelvetri et al., 2013). Since microtubule stability is required for efficient axonal transport (Kapitein and Hoogenraad, 2015), drugs that target microtubule acetylation may be useful candidates to improve the neuropathological presentation of KD. As such, we explored whether ACY-738 was able to stabilize the microtubule cytoskeleton and increase the axonal transport of Twitcher DRG neurons. We started by analyzing microtubule dynamics of Twitcher DRG neurons in the presence of ACY-738. Both in the growth cone and in the axon shaft, ACY-738 decreased microtubule
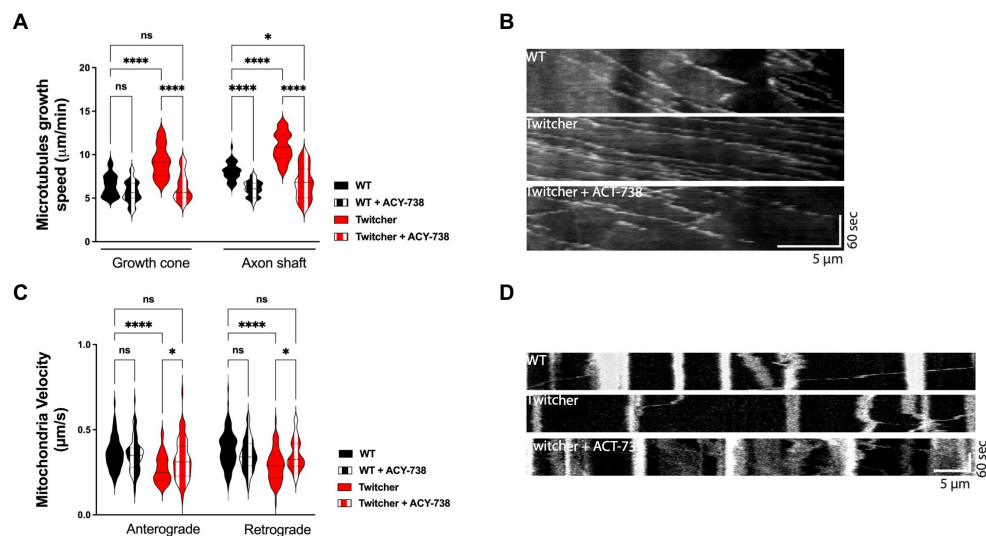
FIGURE 2

In vitro study on the effect of ACY-738 on microtubule dynamics and axonal transport. **(A)** Quantification of microtubule growth speed of WT and Twitcher DRG neurons untreated and treated with ACY-738. Data represent mean $\pm$ SEM (*$p < 0.05$, ****$p < 0.0001$, one-way ANOVA followed by Tukey's multiple comparison test, 22–49 growth cones per condition). **(B)** Kymographs depicting the movement of EB3-GFP in WT and Twitcher DRG neurons untreated and treated with ACY-738. **(C)** Velocity of mitochondria transport of WT and Twitcher DRG neurons isolated from animals either untreated or treated with ACY-738 from P0 until humane endpoints (Twitcher) or similar age ranges (WT). **(D)** Kymographs depicting the movement of mitochondria in WT and Twitcher DRG neurons untreated and treated with ACY-738. Data represent mean $\pm$ SEM (*$p < 0.05$, ****$p < 0.0001$, one-way ANOVA followed by Šidák's multiple comparisons test, 15–76 mitochondria per animal) of $n = 4$ control WT mice, $n = 4$ ACY-738-treated WT mice, $n = 4$ control Twitcher and $n = 3$ ACY-738-treated Twitcher.

growth speed of treated Twitcher DRG neurons (Figures 2A,B) while in treated WT this effect was restricted to the axon shaft, supporting the powerful role of ACY-738 in stabilizing the microtubule cytoskeleton. As previously reported (Teixeira et al., 2014), Twitcher neurons exhibited a higher microtubule growth speed comparing with WT neurons, which was rescued by the treatment with ACY-738 (Figures 2A,B). Of note, no differences were observed in EB3 comet density (data not shown).

As axonal transport efficiency is highly influenced by microtubule organization and dynamics (Kapitein and Hoogenraad, 2015), we hypothesized that the disruption of axonal transport observed in Twitcher mice might be recovered by ACY-738 treatment. In DRG from animals treated until humane endpoints, in agreement with previous reports (Cantuti Castelvetri et al., 2013; Teixeira et al., 2014), Twitcher DRG neurons exhibited a decreased mitochondria velocity both in the anterograde and retrograde direction that was reverted by ACY-738 treatment to the WT levels (Figures 2C,D). ACY-738-treatment did not interfere with the axonal transport of mitochondria in WT animals (Figure 2C). Overall, our data show that ACY-738 is a valuable cytoskeleton-targeting drug to correct defects in microtubule cytoskeleton dynamics and rescue the impaired mitochondrial axonal transport of Twitcher DRG neurons.

3.3. Twitcher mice treated with ACY-738 have improved functional performance

Twitcher mice develop tremors at around 18–20 days of age and muscle weakness and weight loss at P20-25 and usually reach the humane endpoints established in our facility (and

recommended by FELASA) at 30–35 days of age. To determine the possible effect of ACY-738 treatment in disease progression, animals were monitored daily for their functional performance. ACY-738-treatment resulted in a substantial improvement of natural (Figure 3A) and provoked behavior (Figure 3B) and in increased activity levels (Figure 3C). The improvement in behavior of Twitcher mice from day 29 onwards was pronounced as animals that did not respond so efficiently to treatment started to reach humane endpoints and the surviving treated animals outperformed the surviving non-treated group. Despite the general improvement in function, mobility and activity induced by ACY-738 treatment, on its own the drug did not result in an amelioration of weight loss (data not shown) nor in an overall increased average lifespan (Figure 3D).

3.4. ACY-738 delivery rescues the early loss of myelinated axons in the Twitcher CNS and PNS

Given the functional improvement of Twitcher mice treated with ACY-738, we further investigated its potential to correct the early neuropathology of this model. In the optic nerve, as previously reported (Teixeira et al., 2014), P9 Twitcher mice exhibited a decreased density of myelinated fibers when compared with WT nerves (Figures 4A,B). Notably, ACY-738 treatment increased the density of myelinated axons of Twitcher mice partially rescuing the defect of Twitcher optic nerves (Figure 4B). Moreover, the decreased myelin thickness in Twitcher mice was rescued by ACY-738 treatment, as determined by g-ratio analysis (Figure 4C). In the case of unmyelinated
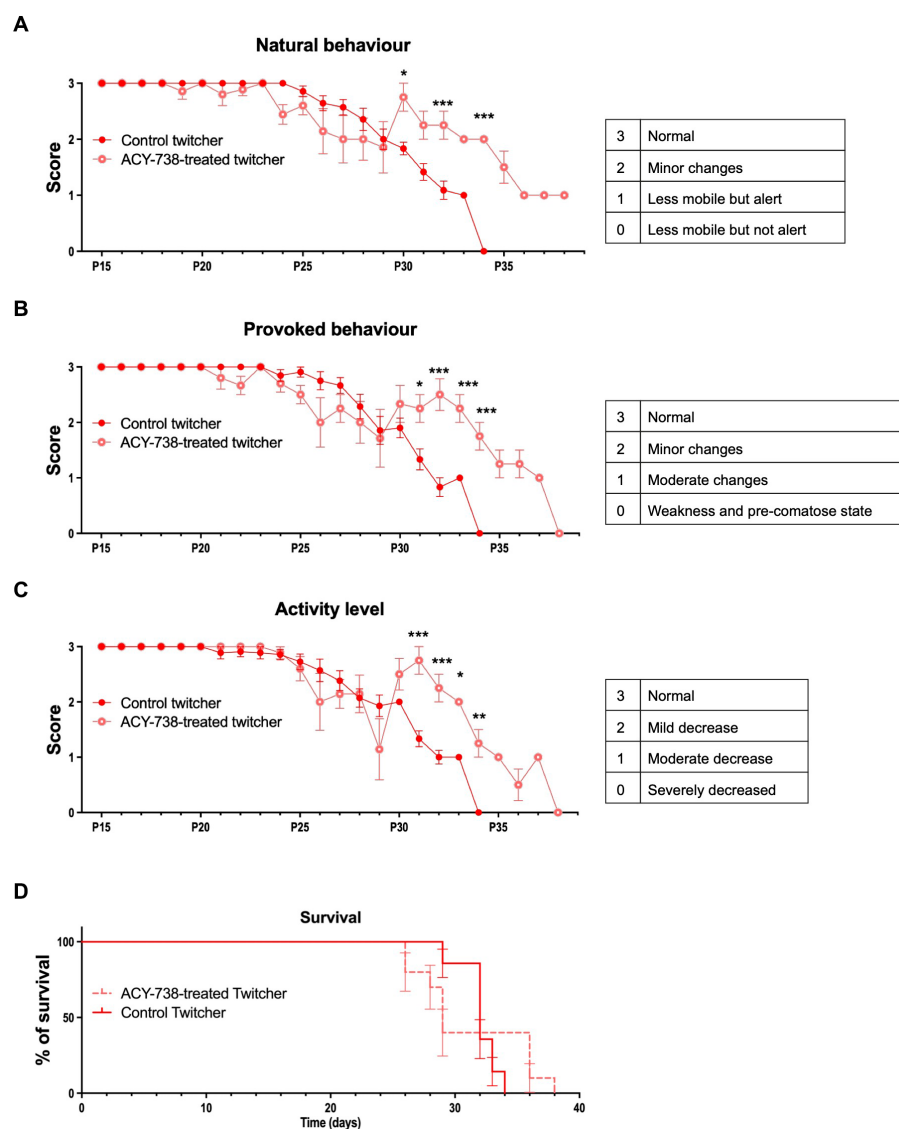
FIGURE 3
Functional analysis of Twitcher mice after ACY-738 treatment. **(A)** Analysis of the natural behavior of Twitcher mice during ACY-738 treatment. Data represent mean $\pm$ SEM (*$p < 0.05$, ***$p < 0.001$, two-way ANOVA) of $n = 14$ control Twitcher and $n = 10$ ACY-738-treated Twitcher. **(B)** Analysis of the provoked behavior of Twitcher mice during ACY-738 treatment. Data represent mean $\pm$ SEM (*$p < 0.05$, ***$p < 0.001$, two-way ANOVA) of $n = 14$ control Twitcher and $n = 10$ ACY-738-treated Twitcher. **(C)** Analysis of the activity level of Twitcher mice during ACY-738 treatment. Data represent mean $\pm$ SEM (*$p < 0.05$, ***$p < 0.001$, two-way ANOVA) of $n = 14$ control Twitcher and $n = 10$ ACY-738-treated Twitcher. Results are only shown starting at P15 as no significant differences were found between treated and untreated animals before that timepoint. **(D)** Kaplan–Meier overall survival curve for control and ACY-738-treated Twitcher mice showing no significant differences between groups (Long-rank test, $p = 0{,}4{,}799$). Each vertical step in the curve indicates one or more deaths (i.e., euthanasia of animals reaching of humane endpoints), data represent mean $\pm$ SEM of $n = 14$ control Twitcher and $n = 10$ ACY-738-treated Twitcher.

axons, their increased density in the optic nerve of Twitcher mice was unchanged by ACY-738 treatment (Figure 4D).

Similar to the optic nerve, P9 Twitcher sciatic nerves displayed a reduced density of both myelinated and unmyelinated axons in comparison with WT sciatic nerves (Figures 4E–H), as previously described by our group (Teixeira et al., 2014). ACY-738 treatment normalized the density of myelinated axons of Twitcher sciatic nerves, as following treatment values were similar to those of WT sciatic nerves (Figure 4F). However, unlike the optic nerve, in the case of the sciatic nerve, ACY-738 treatment did not rescue the decreased myelin thickness (Figure 4G). Similar to the optic nerve, ACY-738 did not rescue the defect of unmyelinated axons in

Twitcher sciatic nerves (Figure 4H). In summary, our data shows that ACY-738 treatment rescues specifically the early loss of myelinated axons in Twitcher mice, both in the CNS (optic nerve) and PNS (sciatic nerve).

3.5. Extended delivery of ACY-738 reverts the optic nerve neuropathology of Twitcher mice

The results obtained from the subcutaneous delivery of ACY-738 from P0-P9 warranted the analysis of treated Twitcher
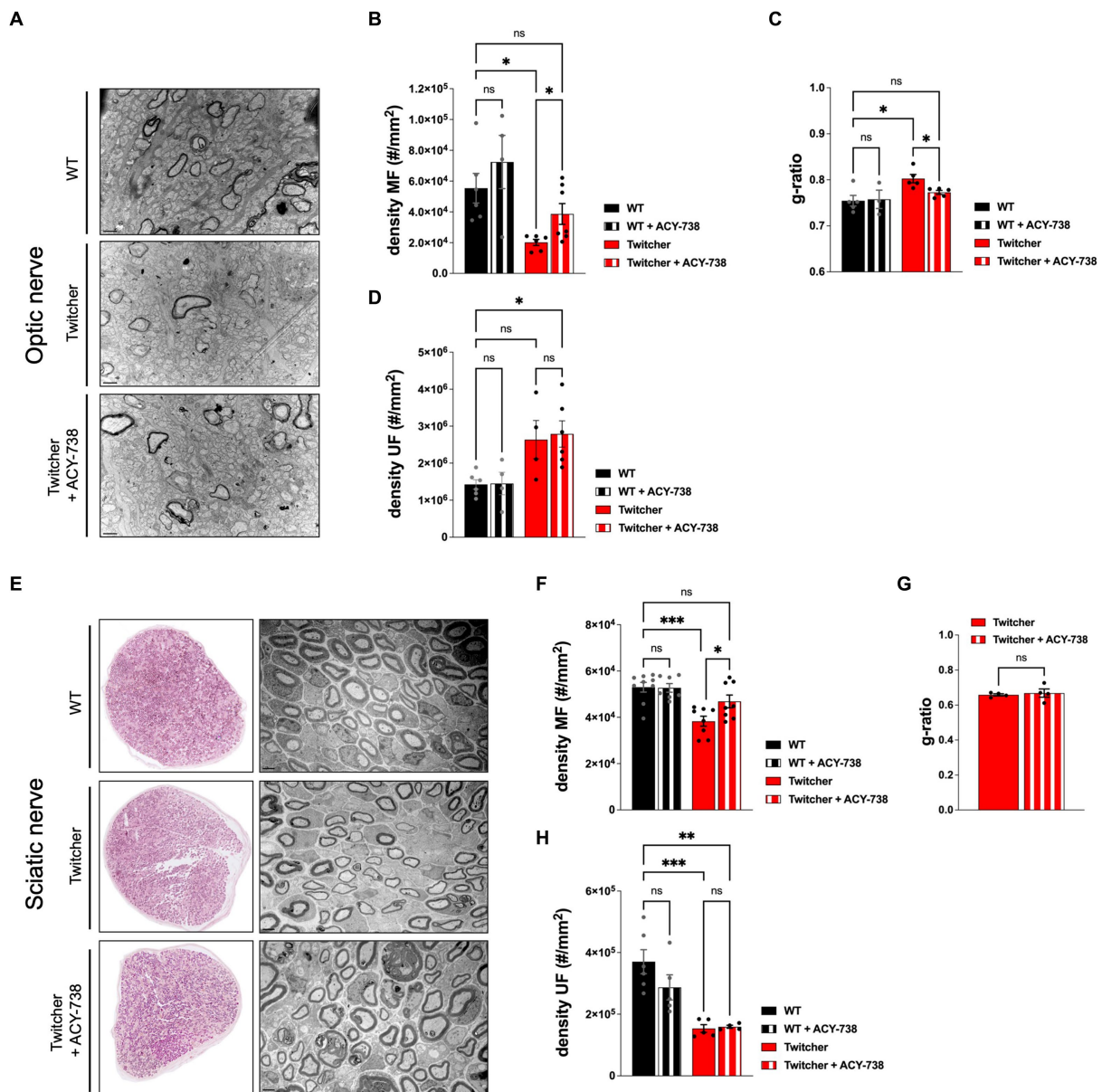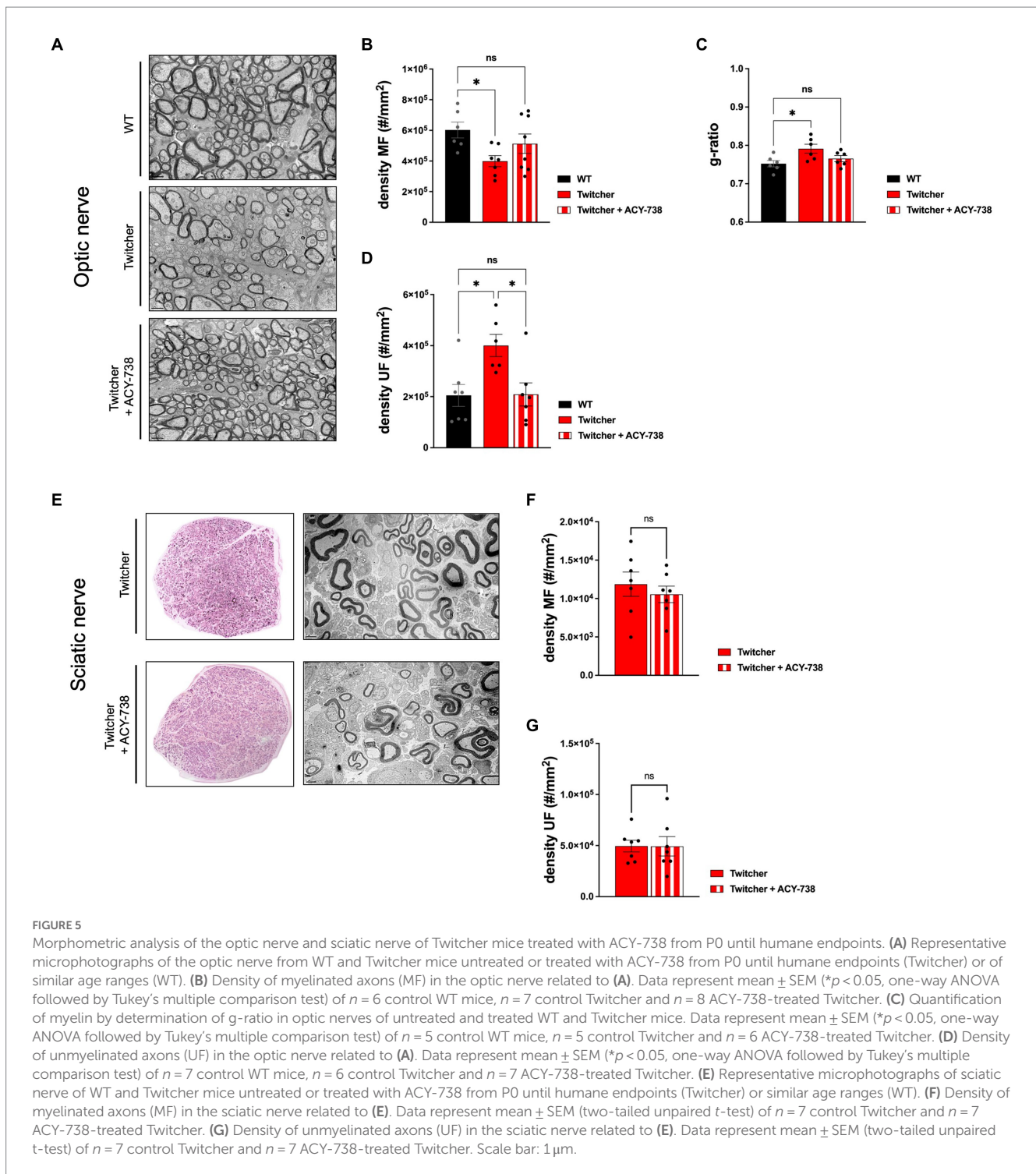
FIGURE 4

Morphometric analysis of the optic and sciatic nerves of P9 WT and Twitcher mice treated with ACY-738. **(A)** Representative microphotographs of optic nerve of P9 WT and Twitcher mice untreated or treated with ACY-738. **(B)** Density of myelinated axons (MF) in the optic nerve related to **(A)**. Data represent mean $\pm$ SEM (*$p < 0.05$, one-way ANOVA followed by Welch's correction) of $n = 7$ control WT mice, $n = 4$ ACY-738-treated WT mice, $n = 8$ control Twitcher and $n = 8$ ACY-738-treated Twitcher. **(C)** Quantification of myelin by determination of g-ratio in optic nerves related to **(A)**. Data represent mean $\pm$ SEM (*$p < 0.05$, one-way ANOVA followed by Welch's correction) of $n = 5$ control WT mice, $n = 3$ ACY-738-treated WT mice, $n = 5$ control Twitcher and $n = 6$ ACY-738-treated Twitcher. **(D)** Density of unmyelinated axons (UF) in the optic nerve related to **(A)**. Data represent mean $\pm$ SEM (*$p < 0.05$, one-way ANOVA followed by Tukey's multiple comparison test) of $n = 6$ control WT mice, $n = 5$ ACY-738-treated WT mice, $n = 4$ control Twitcher and $n = 6$ ACY-738-treated Twitcher. **(E)** Representative microphotographs of sciatic nerve of P9 WT and Twitcher mice untreated or treated with ACY-738. **(F)** Density of myelinated axons (MF) in the sciatic nerve related to **(E)**. Data represent mean $\pm$ SEM (*$p < 0.05$, ***$p < 0.001$, one-way ANOVA followed by Holm–Šídák's multiple comparisons test) of $n = 9$ control WT mice, $n = 7$ ACY-738-treated WT mice, $n = 8$ control Twitcher and $n = 8$ ACY-738-treated Twitcher. **(G)** Quantification of myelin by determination of g-ratio in sciatic nerves related to **(E)**. Data represent mean $\pm$ SEM (two-tailed unpaired t-test) of $n = 4$ control Twitcher and $n = 4$ ACY-738-treated Twitcher. **(H)** Density of unmyelinated axons (UF) in the sciatic nerve related to **(E)**. Data represent mean $\pm$ SEM (**$p < 0.01$, ***$p < 0.001$, one-way ANOVA followed by Holm–Šídák's multiple comparisons test) of $n = 6$ control WT mice, $n = 5$ ACY-738-treated WT mice, $n = 5$ control Twitcher and $n = 4$ ACY-738-treated Twitcher. Data represent mean $\pm$ SEM of $n = 4$ control Twitcher and $n = 4$ ACY-738-treated Twitcher. Scale bar: 1 μm.

mice for extended time periods, i.e., until humane endpoints were reached. Detailed analysis of control and ACY-738-treated Twitcher mice showed that the number of small caliber myelinated axons was increased by ACY-738 treatment (Figure 5A).

Specifically, ACY-738 treatment resulted in a partial rescue of the density of myelinated axons in the optic nerve to the levels of those observed in WT animals (Figures 5A,B). Myelin thickness in Twitcher optic nerves was decreased in comparison with WT,

FIGURE 5
Morphometric analysis of the optic nerve and sciatic nerve of Twitcher mice treated with ACY-738 from P0 until humane endpoints. **(A)** Representative microphotographs of the optic nerve from WT and Twitcher mice untreated or treated with ACY-738 from P0 until humane endpoints (Twitcher) or of similar age ranges (WT). **(B)** Density of myelinated axons (MF) in the optic nerve related to **(A)**. Data represent mean $\pm$ SEM (*$p < 0.05$, one-way ANOVA followed by Tukey's multiple comparison test) of $n = 6$ control WT mice, $n = 7$ control Twitcher and $n = 8$ ACY-738-treated Twitcher. **(C)** Quantification of myelin by determination of g-ratio in optic nerves of untreated and treated WT and Twitcher mice. Data represent mean $\pm$ SEM (*$p < 0.05$, one-way ANOVA followed by Tukey's multiple comparison test) of $n = 5$ control WT mice, $n = 5$ control Twitcher and $n = 6$ ACY-738-treated Twitcher. **(D)** Density of unmyelinated axons (UF) in the optic nerve related to **(A)**. Data represent mean $\pm$ SEM (*$p < 0.05$, one-way ANOVA followed by Tukey's multiple comparison test) of $n = 7$ control WT mice, $n = 6$ control Twitcher and $n = 7$ ACY-738-treated Twitcher. **(E)** Representative microphotographs of sciatic nerve of WT and Twitcher mice untreated or treated with ACY-738 from P0 until humane endpoints (Twitcher) or similar age ranges (WT). **(F)** Density of myelinated axons (MF) in the sciatic nerve related to **(E)**. Data represent mean $\pm$ SEM (two-tailed unpaired t-test) of $n = 7$ control Twitcher and $n = 7$ ACY-738-treated Twitcher. **(G)** Density of unmyelinated axons (UF) in the sciatic nerve related to **(E)**. Data represent mean $\pm$ SEM (two-tailed unpaired t-test) of $n = 7$ control Twitcher and $n = 7$ ACY-738-treated Twitcher. Scale bar: 1 μm.

a defect that was attenuated upon ACY-738 delivery (Figure 5C). Interestingly, with longer delivery times, ACY-738 was able to revert the high density of unmyelinated axons of Twitcher mice, to that observed in WT optic nerves (Figure 5D). In Twitcher sciatic nerves, despite the benefits at early time points post-delivery, the density of both myelinated (Figures 5E,F) and unmyelinated axons (Figure 5G) was unchanged by ACY-738 treatment. Together our data shows that the delivery of ACY-738 to Twitcher mice up to human endpoints is capable of reverting

the neuropathology in the optic nerve whereas the sciatic nerve correction is not achieved.

4. Discussion

KD is a severe neurological condition for which therapeutic options are still limited and mainly focused on managing symptomatology. Even in successful cases, following the current

standard therapy, HSCT, some patients still develop severe peripheral neuropathy years after transplantation (Siddiqi et al., 2006; Wright et al., 2017). In the case of AAV-mediated delivery of *Galc*, in long-term surviving AAV-treated Twitcher mice, multiple demyelinating areas are still detected in the brain, suggesting a possible late onset reduction of AAV efficacy (Rafi et al., 2012, 2015; Heller et al., 2021). As such, the current data on KD strongly points towards the possibility that long-term effective therapies targeting different aspects of the pathology and different groups of patients, will most probably rely on combinatorial approaches.

The knowledge gained on the dysregulated molecular events in KD neurons, specifically on the defects in tubulin acetylation, microtubule dynamics and axonal transport, opens exciting new windows of action to counteract the associated neuropathology. In view of the therapeutic properties of ACY-738 in conditions that share similar pathological features to Krabbe disease, as is the case of demyelinating conditions such as Charcot–Marie Tooth disease and multiple sclerosis where it slows disease progression (LoPresti, 2019) and improves nerve conduction (Benoy et al., 2017), ACY-738 emerged as a promising candidate to test in Krabbe. In fact, our data supports that the positive effects of ACY-738 extend to other conditions where myelin is affected, as is the case of leukodystrophies. Likewise, in the Krabbe disease mouse model, we observed similar outcomes on the improvement of axonal transport, as those previously reported for mouse models of amyotrophic lateral sclerosis (Rossaert et al., 2019; Burg et al., 2021) and Alzheimer disease' (Majid et al., 2015). However, and given the genetic nature of Krabbe disease where toxic substrates of GALC continuously accumulate in the nervous system, ACY-738 did not provide on its own for increased lifespan in this disorder, in contrast to what happens in models of other neurodegenerative diseases (Rossaert et al., 2019; Burg et al., 2021). Still, considering its properties and neuroprotective effects, ACY-738 is a compelling add-on therapeutic candidate for Krabbe disease as it is able to correct the defects on tubulin acetylation, microtubule dynamics and axonal transport and to counteract the early axonal loss observed in Twitcher mice. The reason why these improvements failed to translate into increased lifespan is most likely due to the fact that ACY-738 does not act directly on the genetic cause of the disease, and therefore does not counteract the continuous deleterious accumulation of psychosine.

Our data therefore supports that while ACY-738 cannot be considered as a single therapeutic candidate for KD, it could potentially be tested in combinatorial approaches where gene/enzyme replacement therapy targeting metabolic correction is done.

Data availability statement

The original contributions presented in the study are included in the article/Supplementary material, further inquiries can be directed to the corresponding authors.

Ethics statement

The animal study was reviewed and approved by i3S Ethical Committee, Instituto de Investigação e Inovação em Saúde (i3S), University of Porto, Porto, Portugal.

Author contributions

MS and JN-R coordinated research. MJ, MS, and JN-R designed the study. SB, PB, MJ, MS, and JN-R analysed experiments. SB, MM, MP, AM, and JN-R performed the experiments. SB, MS, and JN-R wrote the manuscript. All authors contributed to the article and approved the submitted version.

Funding

Acknowledgments

Conflict of interest

OG and MJ were employed by Acetylon Pharmaceuticals Inc.

The remaining authors declare that the research was conducted in the absence of any commercial or financial relationships that could be construed as a potential conflict of interest.

Publisher's note

All claims expressed in this article are solely those of the authors and do not necessarily represent those of their affiliated organizations, or those of the publisher, the editors and the reviewers. Any product that may be evaluated in this article, or claim that may be made by its manufacturer, is not guaranteed or endorsed by the publisher.

Supplementary material

The Supplementary material for this article can be found online at: https://www.frontiersin.org/articles/10.3389/fnmol.2023.1231659/full#supplementary-material

SUPPLEMENTARY FIGURE S1
Western blot analysis of tissues from WT and Twitcher mice treated with ACY-738 from P0 until P9. Western blot analysis of tyrosinated tubulin and α-tubulin in **(A)** sciatic nerves and **(B)** optic nerves of P9 Twitcher mice untreated or treated with ACY-738 (upper panels) and respective quantifications (lower panels). Data represent mean $\pm$ SEM (*$p < 0.05$, two-tailed unpaired t-test) of n = 6-8 control Twitcher and n = 9 ACY-738-treated Twitcher.

References

Benoy, V., Vanden Berghe, P., Jarpe, M., Van Damme, P., Robberecht, W., and Van Den Bosch, L. (2017). Development of improved HDAC6 inhibitors as pharmacological therapy for axonal Charcot-Marie-tooth disease. *Neurotherapeutics* 14, 417–428. doi: 10.1007/s13311-016-0501-z

Bradbury, A. M., Bongarzone, E. R., and Sands, M. S. (2021). Krabbe disease: new hope for an old disease. *Neurosci. Lett.* 752:135841. doi: 10.1016/j.neulet.2021.135841

Brites, P., and Sousa, M. M. (2022). Neurons contribute to pathology in a mouse model of Krabbe disease in a cell-autonomous manner. *PLoS Biol.* 20:e3001706. doi: 10.1371/journal.pbio.3001706

Burg, T., Rossaert, E., Moisse, M., Van Damme, P., and Van Den Bosch, L. (2021). Histone deacetylase inhibition regulates lipid homeostasis in a mouse model of amyotrophic lateral sclerosis. *Int. J. Mol. Sci.* 22:11224. doi: 10.3390/ijms222011224

Cantuti Castelvetri, L., Givogri, M. I., Hebert, A., Smith, B., Song, Y., Kaminska, A., et al. (2013). The sphingolipid psychosine inhibits fast axonal transport in Krabbe disease by activation of GSK3beta and deregulation of molecular motors. *J. Neurosci.* 33, 10048–10056. doi: 10.1523/JNEUROSCI.0217-13.2013

Castelvetri, L. C., Givogri, M. I., Zhu, H., Smith, B., Lopez-Rosas, A., Qiu, X., et al. (2011). Axonopathy is a compounding factor in the pathogenesis of Krabbe disease. *Acta Neuropathol.* 122, 35–48. doi: 10.1007/s00401-011-0814-2

Chen, S., Owens, G. C., Makarenkova, H., and Edelman, D. B. (2010). HDAC6 regulates mitochondrial transport in hippocampal neurons. *PLoS One* 5:e10848. doi: 10.1371/journal.pone.0010848

Da Silva, T. F., Eira, J., Lopes, A. T., Malheiro, A. R., Sousa, V., Luoma, A., et al. (2014). Peripheral nervous system plasmalogens regulate Schwann cell differentiation and myelination. *J. Clin. Invest.* 124, 2560–2570. doi: 10.1172/JCI72063

Dompierre, J. P., Godin, J. D., Charrin, B. C., Cordelieres, F. P., King, S. J., Humbert, S., et al. (2007). Histone deacetylase 6 inhibition compensates for the transport deficit in Huntington's disease by increasing tubulin acetylation. *J. Neurosci.* 27, 3571–3583. doi: 10.1523/JNEUROSCI.0037-07.2007

Escolar, M. L., Poe, M. D., Provenzale, J. M., Richards, K. C., Allison, J., Wood, S., et al. (2005). Transplantation of umbilical-cord blood in babies with infantile Krabbe's disease. *N. Engl. J. Med.* 352, 2069–2081. doi: 10.1056/NEJMoa042604

Guo, W., Naujock, M., Fumagalli, L., Vandoorne, T., Baatsen, P., Boon, R., et al. (2017). HDAC6 inhibition reverses axonal transport defects in motor neurons derived from FUS-ALS patients. *Nat. Commun.* 8:861. doi: 10.1038/s41467-017-00911-y

Hagberg, B., Kollberg, H., Sourander, P., and Akesson, H. O. (1969). Infantile globoid cell leucodystrophy (Krabbe's disease). A clinical and genetic study of 32 Swedish cases 1953--1967. *Neuropadiatrie* 1, 74–88. doi: 10.1055/s-0028-1091865

Heller, G., Bradbury, A. M., Sands, M. S., and Bongarzone, E. R. (2023). Preclinical studies in Krabbe disease: a model for the investigation of novel combination therapies for lysosomal storage diseases. *Mol. Ther.* 31, 7–23. doi: 10.1016/j.ymthe.2022.09.017

Heller, G. J., Marshall, M. S., Issa, Y., Marshall, J. N., Nguyen, D., Rue, E., et al. (2021). Waning efficacy in a long-term AAV-mediated gene therapy study in the murine model of Krabbe disease. *Mol. Ther.* 29, 1883–1902. doi: 10.1016/j.ymthe.2021.01.026

Hubbert, C., Guardiola, A., Shao, R., Kawaguchi, Y., Ito, A., Nixon, A., et al. (2002). HDAC6 is a microtubule-associated deacetylase. *Nature* 417, 455–458. doi: 10.1038/417455a

Igisu, H., and Suzuki, K. (1984). Progressive accumulation of toxic metabolite in a genetic leukodystrophy. *Science* 224, 753–755. doi: 10.1126/science.6719111

Jian, W., Wei, X., Chen, L., Wang, Z., Sun, Y., Zhu, S., et al. (2017). Inhibition of HDAC6 increases acetylation of peroxiredoxin1/2 and ameliorates 6-OHDA induced dopaminergic injury. *Neurosci. Lett.* 658, 114–120. doi: 10.1016/j.neulet.2017.08.029

Jochems, J., Boulden, J., Lee, B. G., Blendy, J. A., Jarpe, M., Mazitschek, R., et al. (2014). Antidepressant-like properties of novel HDAC6-selective inhibitors with improved brain bioavailability. *Neuropsychopharmacology* 39, 389–400. doi: 10.1038/npp.2013.207

Kapitein, L. C., and Hoogenraad, C. C. (2015). Building the neuronal microtubule cytoskeleton. *Neuron* 87, 492–506. doi: 10.1016/j.neuron.2015.05.046

Kofler, J., Beltran-Quintero, M. L., Rugari, A., Zuccoli, G., Klotz, S., and Escolar, M. L. (2022). Improved brain pathology and progressive peripheral neuropathy in a 15 year old survivor of infantile Krabbe disease treated with umbilical cord transplantation. *Front. Mol. Neurosci.* 15:888231. doi: 10.3389/fnmol.2022.888231

Krabbe, K. (1916). A new familial, infantile form of diffuse brain-sclerosis. *Brain* 39, 74–114. doi: 10.1093/brain/39.1-2.74

Kreher, C., Favret, J., Weinstock, N. I., Maulik, M., Hong, X., Gelb, M. H., et al. (2022). Neuron-specific ablation of the Krabbe disease gene galactosylceramidase in mice results in neurodegeneration. *PLoS Biol.* 20:e3001661. doi: 10.1371/journal.pbio.3001661

Lee, W. C., Tsoi, Y. K., Dickey, C. A., Delucia, M. W., Dickson, D. W., and Eckman, C. B. (2006). Suppression of galactosylceramidase (GALC) expression in the twitcher mouse model of globoid cell leukodystrophy (GLD) is caused by nonsense-mediated mRNA decay (NMD). *Neurobiol. Dis.* 23, 273–280. doi: 10.1016/j.nbd.2006.03.005

LoPresti, P. (2019). The selective HDAC6 inhibitor ACY-738 impacts memory and disease regulation in an animal model of multiple sclerosis. *Front. Neurol.* 10:519. doi: 10.3389/fneur.2019.00519

Majid, T., Griffin, D., Criss, Z., 2NDJarpe, M., and Pautler, R. G. (2015). Pharmacologic treatment with histone deacetylase 6 inhibitor (ACY-738) recovers Alzheimer's disease phenotype in amyloid precursor protein/presenilin 1 (APP/PS1) mice. *Alzheimers Dement (NY)* 1, 170–181. doi: 10.1016/j.trci.2015.08.001

Miyatake, T., and Suzuki, K. (1972). Globoid cell leukodystrophy: additional deficiency of psychosine galactosidase. *Biochem. Biophys. Res. Commun.* 48, 539–543.

Nogueira-Rodrigues, J., Brites, P., and Sousa, M. M. (2016). Axonal pathology in Krabbe's disease: the cytoskeleton as an emerging therapeutic target. *J. Neurosci. Res.* 94, 1037–1041. doi: 10.1002/jnr.23771

Rafi, M. A., Rao, H. Z., Luzi, P., Curtis, M. T., and Wenger, D. A. (2012). Extended normal life after AAVrh10-mediated gene therapy in the mouse model of Krabbe disease. *Mol. Ther.* 20, 2031–2042. doi: 10.1038/mt.2012.153

Rafi, M. A., Rao, H. Z., Luzi, P., and Wenger, D. A. (2015). Long-term improvements in lifespan and pathology in CNS and PNS after BMT plus one intravenous injection of AAVrh10-GALC in Twitcher mice. *Mol. Ther.* 23, 1681–1690. doi: 10.1038/mt.2015.145

Rivieccio, M. A., Brochier, C., Willis, D. E., Walker, B. A., D'annibale, M. A., Mclaughlin, K., et al. (2009). HDAC6 is a target for protection and regeneration following injury in the nervous system. *Proc. Natl. Acad. Sci. U. S. A.* 106, 19599–19604. doi: 10.1073/pnas.0907935106

Rossaert, E., Pollari, E., Jaspers, T., Van Helleputte, L., Jarpe, M., Van Damme, P., et al. (2019). Restoration of histone acetylation ameliorates disease and metabolic abnormalities in a FUS mouse model. *Acta Neuropathol. Commun.* 7:107. doi: 10.1186/s40478-019-0750-2

Sakai, N., Inui, K., Tatsumi, N., Fukushima, H., Nishigaki, T., Taniike, M., et al. (1996). Molecular cloning and expression of cDNA for murine galactocerebrosidase and mutation analysis of the twitcher mouse, a model of Krabbe's disease. *J. Neurochem.* 66, 1118–1124. doi: 10.1046/j.1471-4159.1996.66031118.x

Siddiqi, Z. A., Sanders, D. B., and Massey, J. M. (2006). Peripheral neuropathy in Krabbe disease: effect of hematopoietic stem cell transplantation. *Neurology* 67, 268–272. doi: 10.1212/01.wnl.0000230156.01228.33

Smith, B., Galbiati, F., Cantuti-Castelvetri, L., Givogri, M. I., Lopez-Rosas, A., and Bongarzone, E. R. (2011). Peripheral neuropathy in the Twitcher mouse involves the activation of axonal caspase 3. *ASN Neuro* 3:art:e00066:AN20110019. doi: 10.1042/AN20110019

Sourander, P., and Olsson, Y. (1968). Peripheral neuropathy in globoid cel leucodystrophy (morbus Krabbe). *Acta Neuropathol.* 11, 69–81. doi: 10.1007/BF00692796

Su, Q., Li, T., He, P. F., Lu, X. C., Yu, Q., Gao, Q. C., et al. (2021). Trichostatin a ameliorates Alzheimer's disease-related pathology and cognitive deficits by increasing albumin expression and Abeta clearance in APP/PS1 mice. *Alzheimers Res. Ther.* 13:7. doi: 10.1186/s13195-020-00746-8

Suzuki, K., and Suzuki, K. (1995). The twitcher mouse: a model for Krabbe disease and for experimental therapies. *Brain Pathol.* 5, 249–258. doi: 10.1111/j.1750-3639.1995.tb00601.x

Tanaka, K., Nagara, H., Kobayashi, T., and Goto, I. (1988). The twitcher mouse: accumulation of galactosylsphingosine and pathology of the sciatic nerve. *Brain Res.* 454, 340–346. doi: 10.1016/0006-8993(88)90835-9

Teixeira, C. A., Miranda, C. O., Sousa, V. F., Santos, T. E., Malheiro, A. R., Solomon, M., et al. (2014). Early axonal loss accompanied by impaired endocytosis, abnormal axonal transport, and decreased microtubule stability occur in the model of Krabbe's disease. *Neurobiol. Dis.* 66, 92–103. doi: 10.1016/j.nbd.2014.02.012

Weinstock, N. I., Shin, D., Dhimal, N., Hong, X., Irons, E. E., Silvestri, N. J., et al. (2020). Macrophages expressing GALC improve peripheral Krabbe disease by a mechanism independent of cross-correction. *Neuron* 107, 65–81.e9. doi: 10.1016/j.neuron.2020.03.031

Wenger, D. A., Rafi, M. A., and Luzi, P. (1997). Molecular genetics of Krabbe disease (globoid cell leukodystrophy): diagnostic and clinical implications. *Hum. Mutat.* 10, 268–279. doi: 10.1002/(SICI)1098-1004(1997)10:4<268::AID-HUMU2>3.0.CO;2-D

White, A. B., Givogri, M. I., Lopez-Rosas, A., Cao, H., Van Breemen, R., Thinakaran, G., et al. (2009). Psychosine accumulates in membrane microdomains in the brain of Krabbe patients, disrupting the raft architecture. *J. Neurosci.* 29, 6068–6077. doi: 10.1523/JNEUROSCI.5597-08.2009

Wright, M. D., Poe, M. D., Derenzo, A., Haldal, S., and Escolar, M. L. (2017). Developmental outcomes of cord blood transplantation for Krabbe disease: a 15-year study. *Neurology* 89, 1365–1372. doi: 10.1212/WNL.0000000000004418

Zaka, M., and Wenger, D. A. (2004). Psychosine-induced apoptosis in a mouse oligodendrocyte progenitor cell line is mediated by caspase activation. *Neurosci. Lett.* 358, 205–209. doi: 10.1016/j.neulet.2003.12.126

Zilberman, Y., Ballestrem, C., Carramusa, L., Mazitschek, R., Khochbin, S., and Bershadsky, A. (2009). Regulation of microtubule dynamics by inhibition of the tubulin deacetylase HDAC6. *J. Cell Sci.* 122, 3531–3541. doi: 10.1242/jcs.046813